# Nile Red lifetime reveals microplastics identity

Giuseppe Sancataldo[1], Giuseppe Avellone[2], Valeria Vetri[1]

[1] Dipartimento di Fisica e Chimica – Emilio Segrè, Università degli Studi di Palermo, Viale delle scienze Edificio 18, 90128 Palermo, Italy

[2] Dipartimento di Scienze e Tecnologie Biologiche Chimiche e Farmaceutiche, Via Archirafi 32, 90123 Palermo

KEYWORDS: microplastics, water pollution identification, nile red, fluorescence lifetime imaging, phasor analysis

ABSTRACT: Microplastics pollution has been recognized as a worldwide environmental problem. The increasing daily use and the release of plastics in the environment have led to the accumulation of fragmented microplastics, with potentially awful consequences to the environment, animal and human health. Detection and identification of microplastics are of utmost importance but still limited.

In this work, a new approach is presented for the analysis of microplastics, based on hydrophobic fluorescent staining of Nile Red, using spectrally resolved confocal fluorescence microscopy and Fluorescence Lifetime Imaging Microscopy (FLIM). Significant differences were observed in the emission spectrum and in the fluorescence lifetime among analyzed microplastics. Nile Red fluorescence shows a sensible behavior according to polymer matrix and provides a fingerprint for the identification of fragments from different types of plastics. Lifetime imaging coupled with a phasor analysis

constitutes a fast, robust and straightforward method to map and identify different microplastics within the same sample in aquatic environment.

TOC:

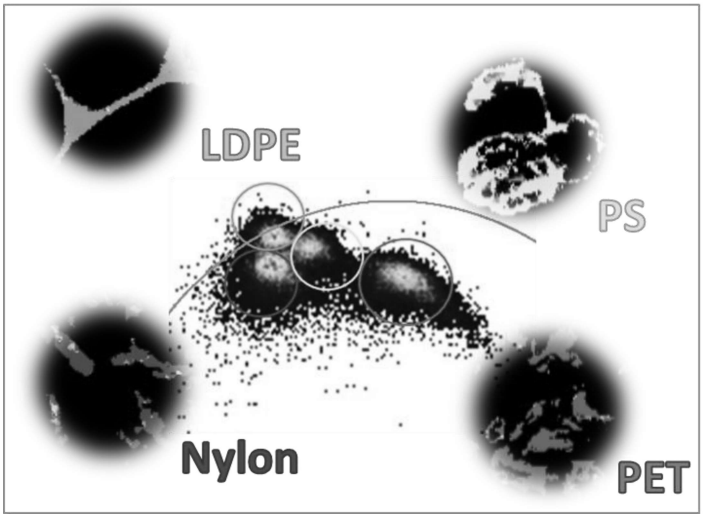


MAIN TEXT

**Introduction.**

Microplastics (MPs) are plastic fragments and fibers whose size ranges from millimeter to nanometer scale, which contaminate the environment being ubiquitous across water, ice, air and land [1–6]. MPs are mainly composed by synthetic polymers whose production and common discharges are continuously increasing [7]. For this reason, MPs are nowadays considered a persistent and problematic form of pollution. Large efforts are being focused in their environmental assessment and in the characterization of their main sources and pathways, this being aimed at identifying measures to reduce their impact on the ecosystems.

Due to the variety of processes that lead to the formation of these small plastic fragments from different materials, a large variety of size and shape progressively evolving can be found [8]. Fragments, fibres, film, foam and pellets were the most frequently reported shapes.

MPs are of increasing ecological concern and are attracting a large interest worldwide from scientific community which is attempting to increase the knowledge about these heterogeneous mixtures of polymers which are becoming a real danger to the ecosystem and as a consequence for human health. MPs are internalized by living organisms ranging from microbial communities, zoo-plankton, crabs to larger fishes [9,10] and they have been found to exert profound biological effects leading to adverse effects on their survival and health [11]. In addition to direct primary effects, it is important to consider that MPs have high specific surface areas and they can easily interact with toxic compounds as heavy metal ions or persistent organic pollutant thereby becoming dangerous contaminants [12,13]. Humans are chronically exposed to micro plastics as they can be ingested and inhaled this possibly representing a serious hazard whose outcome still have to be clearly defined [14–16]. The inherent toxicity of MPs may vary with their size [17,18] and composition and exposed functional groups which may lead to different toxic effects and act in combination with the chemical compound they absorb [19]. For example size dependent and synergistic effects with Au were reported for polystyrene in zebrafish [18], moreover, different MPs were found to increase or reduce Nickel toxicity in the water flea D. magna [20]. This last together with others results [21,22] suggest a relevant role of physicochemical characteristics of micro particles.

In the last years an increasing number of studies has evidenced the need of detailed characterization of the microplastics samples after collection from water [23–26]. In order

63 to get a comprehensive knowledge of the impact that MPs may have in our future,
64 quantitative methods are needed to characterize different particles in different matrices
65 able to univocally distinguish different species in the samples reporting their shape,
66 polymer type and particles size in different environments. Straightforward, low time-
67 consuming methods minimally invasive are largely desired which may allow to map and
68 quantitatively characterize this heterogeneous system.

69 Traditionally MPs are characterized visually by naked eye or by means of optical
70 microscopy describing morphological properties [9,27,28] this may hinder results due to
71 the lack of reliable identification. In this context, the application of spectroscopies (Mass
72 spectroscopy, infrared and Raman spectroscopy) or tailored thermos-analytical methods
73 for the identification and quantification of MPs had led to a substantial increase of
74 specificity allowing gaining important information on sample chemical composition
75 [23,29–32]. A further advantage is found in the combination of spectroscopy and
76 microscopy techniques [33]. FTIR/Raman microscopies had large impact on this research
77 as they are nondestructive methods allowing the identification of polymer types,
78 pollutants and modifications due to environmental conditions, particles number,
79 morphology and size [29,30]. FTIR/Raman microscopy provides a useful fingerprints of
80 the different plastics via the analysis of vibrational absorption but, even if considering
81 established libraries and automated spectral matching, it is error prone, especially for
82 small particles (<20 μm) where microscope resolution includes spectral signals from the
83 surroundings limiting the identification of particles of smaller size.

84 The exquisite sensitivity of fluorescence, in this context, could be largely applied for the
85 identification and characterization of MPs. Although this technique does not provide
86 direct structural and chemical information, it acquires a noteworthy relevance if external

87 fluorescent dyes are used. In particular for those dyes whose spectral properties critically
88 change depending on the interaction with the host environment. Fluorescence microscopy
89 can be applied to obtain size and shape information for microparticles down to the
90 nanometric scale (using super-resolution techniques) simultaneously giving information
91 on their composition, presence of pollutants and their interaction with the environment
92 [34,35]. A large variety of fluorescent molecules, indeed, exist whose signal reports for
93 specific interactions, for the polarity or the rigidity of molecular environment, the
94 presence of metal ions, pH or temperature, ionic strength, dielectric constant, presence
95 and concentration of peculiar groups, analytes effects and the presence a specific target
96 can be detected even in traces [36]. Few systematic studies have been reported on the
97 possibility of apply this method mainly focused on the hydrophobic dye Nile Red (9-
98 diethylamino-5H-benzo[a]phenoxazine-5-one) [37–42], which efficiently stains surface
99 of microplastics, facilitating their detection. This dye is widely used in biophysical studies
100 focusing in proteins, lipids and live cell analysis [43,44]. Depending on the environment,
101 Nile Red exhibits different absorption and fluorescence spectra, quantum yields, and
102 fluorescence lifetimes. Specifically, in organic solvent or in apolar environment it gives
103 a strong fluorescence which changes according to the environment, presenting an
104 emission blue shifts in nonpolar environments [45].

105 Nile-red may be used to distinguish MPs according to their hydrophobicity as its spectrum
106 undergoes large shifts according to it, specific spectral changes can be also used to assess
107 various plastics modification following different environmental aggressions (UV
108 exposure, oxidation, thermally induced modifications and so on). Nile Red was also used
109 for model studies in polymers, probing differences in micropolarity in PMMA and PVA
110 films, interestingly fluorescence lifetime of this molecule was proposed as a tool to
111 estimate plastic's Young modules [46]. A group of studies demonstrated that Nile Red

staining can be used for fast automated methods to identify MPs (hundreds micron range) using wide field fluorescence microscopy in water and in sediments [41,47]. These methods were found to have large efficiency offering an important screening step before other more detailed analysis. Due to advantages of this method also co-staining was tested broadening characterization possibilities and highlighting the possibility to increase the accuracy [48]. The large amount of studies on spectroscopic properties of Nile Red in different environments ranging from multiple organic solvents, proteins, lipids, live cells to $TiO_2$ matrices [49] provide a strong background to build solid description of heterogeneous systems like MPs. The coupling of microscopy and spectral analysis in addition may provide information on the nature of the interaction between the dye, whose fluorescence mechanisms are well assessed, and its microenvironment lighting on the nature of the MPs.

In this work, we present the analysis of Nile Red stained MPs using confocal fluorescence microscopy and Fluorescence Lifetime Imaging Microscopy (FLIM). We analyzed the emission spectra acquired at the microscope of low-density polyethylene (LDPE), polystyrene (PS), polyethylene terephthalate (PET), and polyamide (Nylon) separating spectral range where large variations occur giving information on different microplastics/dye coupling. In addition, FLIM allows mapping Nile Red fluorescence lifetime producing images, which encode information about the spatial distribution the stained sample together with information about the nano-environment of the dye.

Nile Red fluorescence lifetime measurement offers an additional parameter, not affected by scattering or dye concentration, that has been proven to report information on the dielectric constant, rigidity, hydrogen bond donating power of the medium [44,46,50].

Importantly, FLIM data are analyzed by means of the Phasor approach [51,52], a fit free, graphical methods which allow mapping at pixel resolution fluorescence lifetime distribution in the image. We highlight that different microplastics are characterized by clearly distinguishable lifetime distributions, which allow separating fluorescent species beyond the spectral options, the results clearly show that different microplastics almost indistinguishable by optical microscopy can be readily separated in a single image. We present proof-of-principle concept of our method using MPs produced from four model plastic types coming from commercial objects of common use, this providing a new platform for the analysis of MPs and their fate in the environment.

## Material and methods.

*Sample preparation.*

Consumer plastics were identified through their recycling symbols. The plastics used were low-density polyethylene (LDPE) recycling code 04, polystyrene (PS) recycling code 06, polyethylene terephthalate (PET) recycling code 01, and polyamide (Nylon) recycling code 07 [53]. Microplastics fragments were prepared cutting/scraping fragments from blocks of commercial virgin plastic. Specifically, 1) LDPE heterogeneous fragments were obtained by cutting a LDPE plastic sheet 2) PS, PET, Nylon fragments were obtained scraping plastic blocks using a hand file tool (USAG990 B PA/200). Samples staining was carried out by adding Nile Red stock solution in deionized water to give a final concentration of 0.5 μM in a suspension of 25 mg/ml of microplastics. Samples were incubated for 2h at 60 °C with vigorous agitation. Sample containing

158 different MPs was obtained by mixing 250 μL solution of each stained sample, no
159 significant differences in MPs fluorescence intensity and lifetime are observed for several
160 hours, or staining the sample after mixing MPs.

161 *Confocal optical microscopy and spectral analysis.*

162 Fluorescence and bright-field optical images were acquired by a Leica TCS SP5 confocal
163 laser scanning microscope, using a 20× air objective (Leica Microsystems, Germany).
164 Leica "white light laser" (repetition frequency 80 MHz) laser was used in order to excite
165 Nile Red ($\lambda_{ex}$=500 nm). Fluorescence emission signal was acquired in the range 520-720
166 nm. Spectral images were acquired in the range 520-720 nm using 10 nm detection range
167 as emission bandwidth. Fluorescence image analysis we performed using Fiji software
168 (https://imagej.net/Fiji). Within the experimental error autofluorescence signal is not
169 observed for MPs sample without staining.

170 *Fluorescence lifetime imaging.*

171 Fluorescence lifetime imaging measurements were acquired in the time domain by a
172 Leica TCS SP5 confocal laser scanning microscope, using a 20× air objective (Leica
173 Microsystems, Germany) equipped with a picoHarp 300 standalone TCSPC module
174 (Picoquant). 256 × 256 pixels images were acquired at a scanning frequency of 400 Hz.
175 Leica "white light" laser was used in order to excite NR ($\lambda_{ex}$=500 nm). Fluorescence
176 emission were spectrally detected in three different channels: $\lambda_{em}$=520-570 nm, $\lambda_{em}$=570-
177 620 nm $\lambda_{em}$=620-670 nm).

178 *FLIM analysis.*

179 FLIM data were analyzed by means of the phasor approach using SimFCS software
180 developed at the Laboratory of Fluorescence Dynamics, University of California at Irvine

(www.lfd.uci.edu). The laser repetition frequency used for calculation of phasors is provided to analysis software by the calibration measurement performed by measuring the known lifetime of the fluorescein in aqueous solution at basic pH that is a single exponential of 4.0 ns.

Phasor analysis is a Fourier domain technique, which allows the transformation of the fluorescence signal from each pixel in the image to a point in the phasor plot. The coordinates g and s (cosine and sine transforms, respectively) of each point in the phasor plot are calculated from the fluorescence-intensity decay in the corresponding pixel in the FLIM image. Each lifetime is mapped in a phasor plot and all possible single exponential lifetimes lie on the "universal circle," defined as the semicircle going from point (0, 0) to point (1, 0), with radius 1/2. Point (1, 0) corresponds to $\tau = 0$, and point (0, 0) to $\tau = \infty$.

**Results and discussion.**

Micro plastics were obtained from commercial products and mechanically fragmented to a microscale size. In Figure 1 representative 1024x1024-pixels optical microscopy measurements are reported for low-density polyethylene (LDPE), polystyrene (PS), polyethylene terephthalate (PET), and polyamide (Nylon) dispersed in water, scale bar is 200 μm.

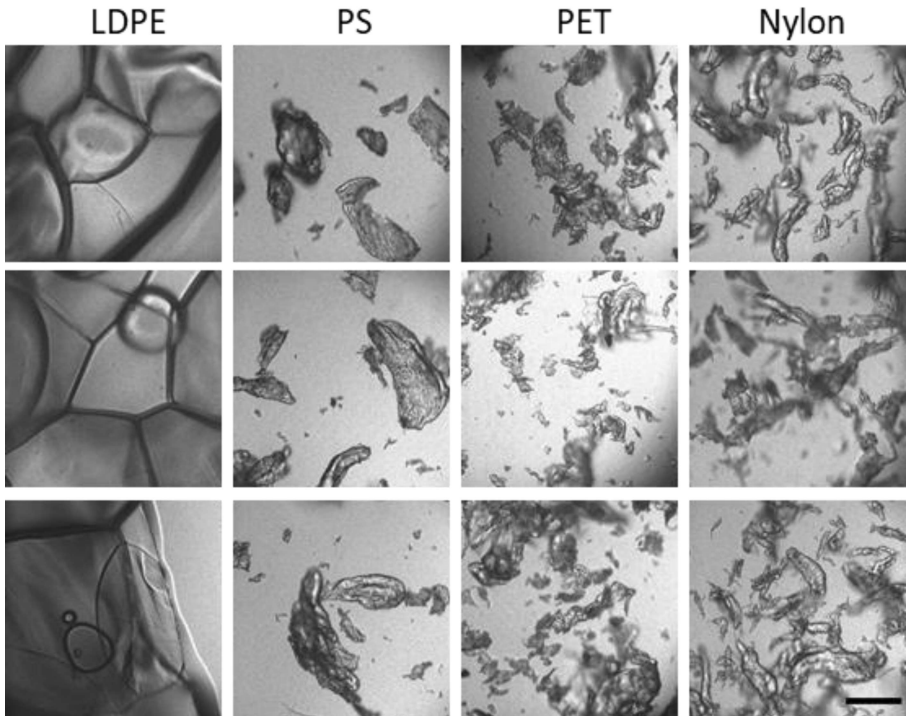


**Figure 1.** *Representative optical images of microplastics dispersed in water. From left to right: low-density polyethylene (LDPE), polystyrene (PS), polyethylene terephthalate (PET), and polyamide (Nylon). Scale bar is 200 µm.*

As can be seen PS, PET and Nylon are characterized by small heterogeneous flakes and chips whose size varies from tens to few hundreds microns, they cannot be distinguished by visual inspection. At difference, LDPE reveals a net like structure.

In Figure 2, we report 1024x1024-pixels representative fluorescence confocal microscopy measurements on the same sample stained with Nile Red as described in the Material and methods section. Images are acquired in the same experimental conditions and in particular using same laser intensity and emission bandwidth. In line with other results in literature LDPE, PS, PET and Nylon are stained at their surface and can be visualized with higher contrast [38,41]. In these samples, heterogeneous distribution of fluorescence

signal seems to indicate not uniform staining, and no significant difference in fluorescence intensity is measured, and again only LDPE can be clearly distinguishable from its morphology.

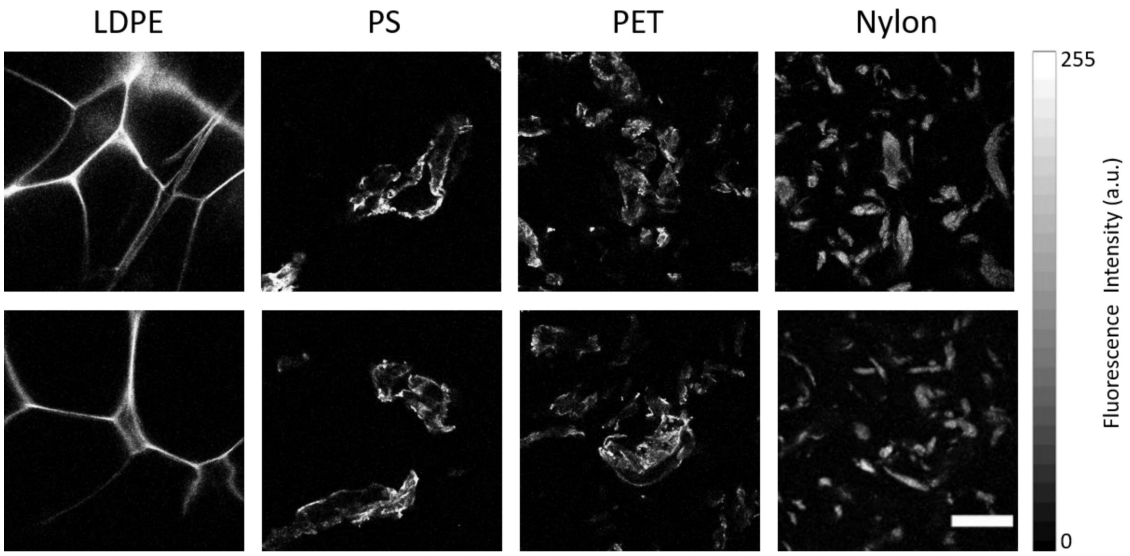


**Figure 2.** *Representative confocal fluorescence microscopy images of microplastics dispersed in water stained with Nile Red. From left to right: low-density polyethylene (LDPE), polystyrene (PS), polyethylene terephthalate (PET), and polyamide (Nylon). Fluorescence emission signal is acquired in the range 520-720 nm using* $\lambda_{ex}$*=500 nm. Scale bar is 200 µm.*

On the same samples, by exciting Nile Red fluorescence under laser light at $\lambda_{exc}$= 500 nm, fluorescence spectra were acquired in the range 520-720 nm using 10 nm detection range as emission bandwidth. Normalized fluorescence spectra and confocal microscopy images at corresponding wavelength intervals are reported in Figure 3.

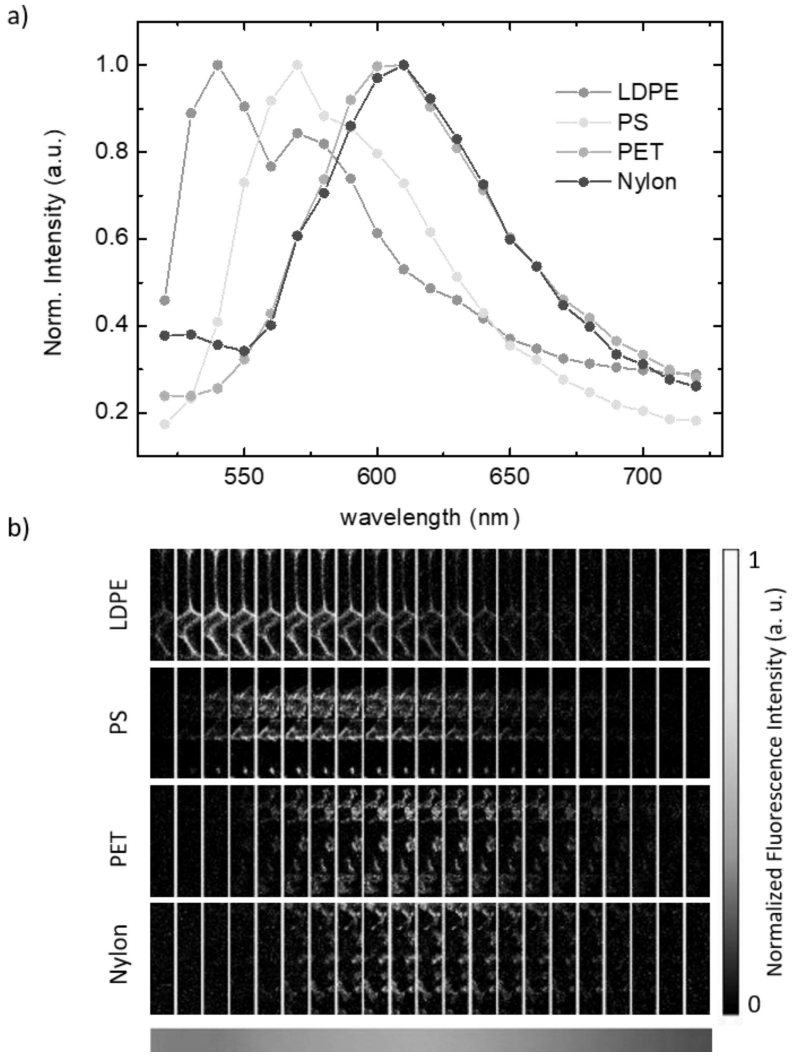


227

228 **Figure 3.** *Nile Red fluorescence spectral analysis of microplastics. Normalized*
229 *fluorescence spectra (a) and normalized microscopy images at corresponding*
230 *wavelength intervals (b). Fluorescence spectra ($\lambda_{exc}$= 500 nm) were acquired in the range*
231 *520-720 nm using 10 nm detection range as emission bandwidth.*

232

233 In both Figure 3a and 3b it is possible to recognize that Nile Red fluorescence emission
234 spectra are progressively red shifted going from LDPE, PS to PET and Nylon. In
235 particular, LDPE presents an intensity maximum at about 545 nm, in PS the emission

peak is shifted to 560 nm while PET and Nylon it almost overlaps being above 600 nm. Only a tiny difference exists between these two last samples consisting in a small shoulder at about 540 nm in Nylon which is not observed in PET. Nile Red adsorbs to the surface of microplastics and give them a slightly different color depending on their composition. Polar polymers like Nylon and PET present a red shifted spectrum with respect to more hydrophobic structure like PS and LDPE. Interestingly, the solvatochromic properties of Nile Red were previously used to measure the local dielectric constant in polymeric films revealing a red shift at increasing dielectric constant (ε) [50]. In our specific case the same effect is observed in line with the literature, indeed reported dielectric constant values for these plastics are about 2.2 for LDPE, between 2.4 and 2.9 for PS, between 3 and 4 for PET and about 4 for Nylon [54]. These measurements reveal the ease of differentiating samples by means of fluorescence microscopy at least grouping them according to specific properties which depend on the molecular structure and that may regulate interactions with the environment.

The origin of the solvatochromic behavior of Nile Red relies on its molecular interaction with the host environment [55]. A Twisted Intramolecular Charge Transfer (TICT) state has been proposed to account for the polarity-sensitive fluorescence of Nile red [55]. As reported in the introduction, molecular coupling with the environment of fluorescent dyes in general is reflected with high sensitivity by time resolved fluorescence measurements. Excited state dynamics provide a further parameter that can be used to detect environmental properties. Specifically, here we use the time resolved fluorescence analysis of Nile Red to detect the specific interaction of Nile Red with different microplastics.

In Figure 4 fluorescence lifetime decays measured in Nile-Red stained LDPE, PS, PET and Nylon samples dispersed in water in 3 different spectral regions are reported a) 520-570 nm b) 570-620 nm c) 620-670 nm. The selected ranges covers the entire Nile Red fluorescence spectrum (see Figure 3a). In particular, the higher a) and lower c) energy ranges correspond to the initially excited state and to the lower energy state attributed to solvent relaxation. In literature, for Nile Red solvent relaxation is attributed to several sources as internal charge transfer, hydrogen bonding, solvent polarity depending on probe environment [36,56].

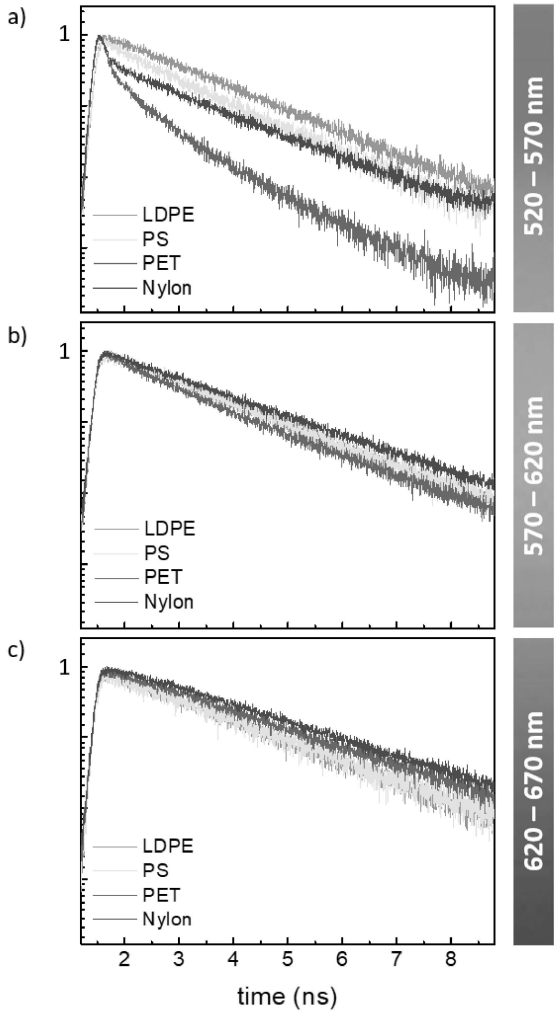

**Figure 4.** *Spectral lifetime analysis of Nile Red stained samples: Fluorescence decays for LDPE, PS, PET and Nylon fragments dispersed in water, measured in three different spectral regions a) 520-570 nm b) 570-620 nm c) 620-670 nm.*

As evident in Figure 4, larger differences in fluorescence decays are observed in the higher energy range (520-570 nm- panel a). In particular, Nile Red fluorescence decay for LDPE sample seems to be well described by a single exponential with the longer lifetime among the observed sample, shorter lifetimes but also more complex decays are observed for PS and Nylon and the faster decay is measured in PET. Smaller differences in fluorescence decays are also detected accordingly in the other ranges. Emission-wavelength-dependent fluorescence intensity decays of Nile Red were previously studied to asses Nile Red fluorescence mechanisms depending on the complexity of the environment. While in pure apolar solvents (as methanol) Nile Red fluorescence shows a single exponential decay at all emission wavelengths, more complex fluorescence decays (at different wavelengths) indicate specific effects of the environment experienced by the dye [38,50]. In the analyzed samples spectral variations of fluorescence decay may arise by different plastic composition also in interaction with the surrounding water. As expected faster decays in the higher energy region (green) are observed in plastics whose steady state emission spectra are red shifted. Presented data clearly show that in this channel lifetime represent a significant observable that can be used to readily distinguish microplastics.

For this reason, in Figure 5 the phasor analysis of FLIM measurements on this spectrally filtered region is reported for Nile Red stained LDPE, PS, PET and Nylon microplastics dispersed in water. Phasor analysis is a graphical method, based on the Fourier transform

292 of fluorescence decays at each pixel of the image [51,52] which does not require any
293 model or fitting procedure. It simplifies the way of analyzing FLIM data and provides a
294 graphical view of lifetime distributions making data interpretation fast and easy.
295 Fluorescence decay lifetimes are graphically mapped in a polar plot (phasor plot) and they
296 can be easily identified by their position at single pixel resolution. This is particularly
297 useful in the case of systems with complex photophysics as Nile Red, whose
298 interpretation and modeling can be really challenging. Every fluorescence decay is
299 represented in a specific location in the phasor plot which can be considered a fingerprint
300 of a particular species. Since its introduction, the phasor analysis has been widely used
301 for the analysis of a wide range of fluorescence molecules [57–59], including Nile-Red
302 [60]. A wide range of systems was analyzed ranging from living organisms, tissues and
303 cells, protein aggregates [61,62] to organic solar cells [63,64]. This method allows both
304 quantitative interpretation of FLIM data, but more importantly to map processes and
305 multiple species.

306 In Figure 5a a representative 256×256-pixels fluorescence intensity map of a Nylon
307 sample is reported. The phasor plot corresponding to these images is reported in Figure
308 5b. As can be seen, lifetime distribution is represented by a cloud of points inside the
309 universal circle indicating that in Nylon microplastics Nile Red decay is characterized by
310 a non-single exponential decay. It is possible to select pixel in the phasor plot by a colored
311 circle and the corresponding pixels characterized by selected lifetime are mapped back in
312 the image using the same color code. In the presented phasor a red circle was used and
313 all pixels in the image at fluorescent structures are red colored (Figure 5c). Supplementary
314 video 1 shows how, after data transformation to the phasor plot, this procedure allows to
315 spatially identify in the image pixel with the same lifetime distribution.

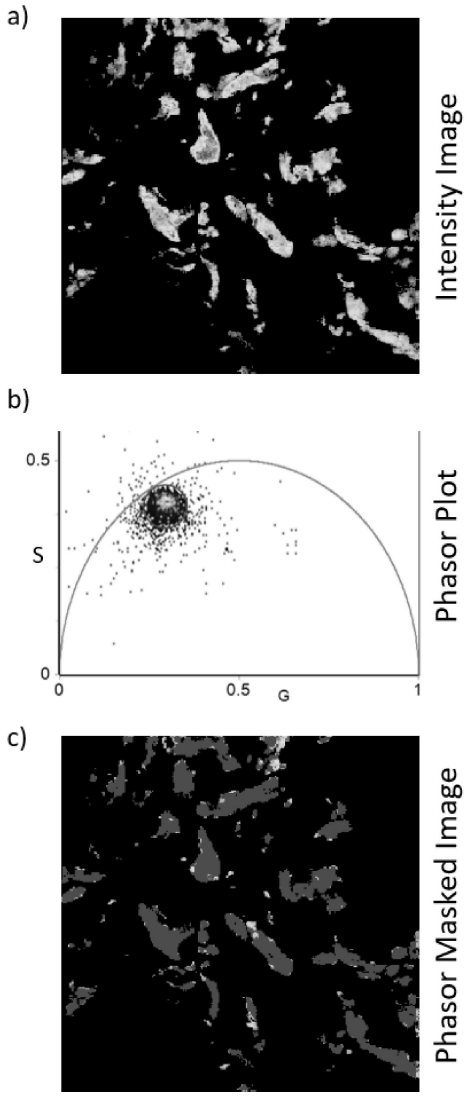


**Figure 5.** *Phasor analysis workflow. Nylon sample is reported as an example. (a) Fluorescence Intensity image, (b) Phasor plot (c) Phasor masked image. Lifetime distribution is represented by a cloud of points in the phasor plot that can be selected by a colored circle (red) and the corresponding pixels characterized by selected lifetime are mapped back in the image using the same color code.*

The simultaneous Phasor analysis of FLIM measurements for LDPE, PS, PET, Nylon is reported in Figure 6. In Panel 6a we report the phasor plot obtained by four different measurements for each plastics and in panel b) the corresponding phasor maps colored according to the selection in the phasor plot.

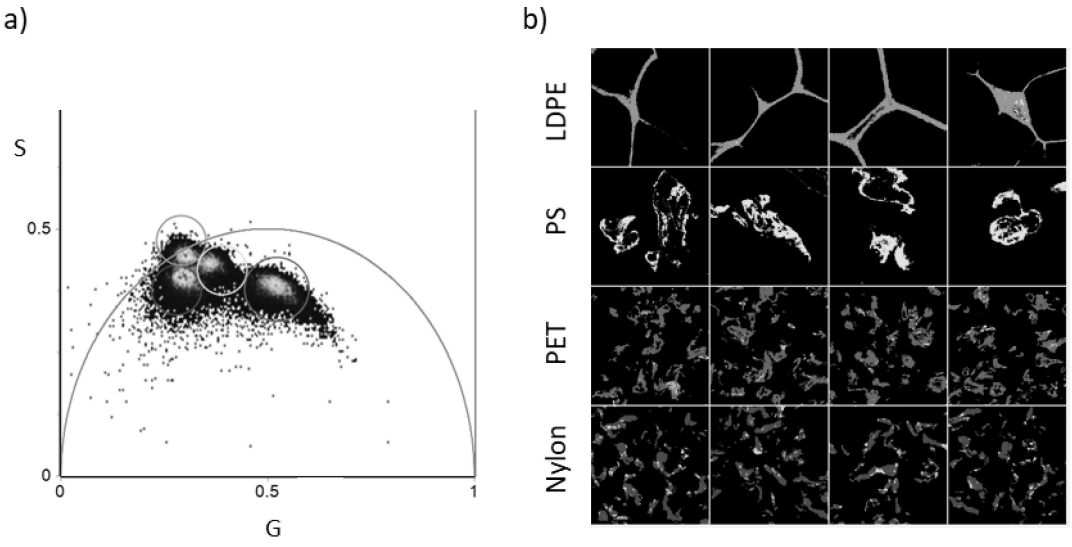


**Figure 6.** *Simultaneous Phasor analysis of FLIM measurements. A) Phasor plot of LDPE, PS, PET and Nylon. For each sample a single cloud of points in the phasor plot is found. b) Phasor color map in which each pixel is colored according to the color of the corresponding cursor in the phasor plot.*

For each sample, a single cloud of points in the phasor plot is found, and importantly, clouds reporting for lifetimes distributions are spatially distinguishable. Corresponding selections are mapped in the phasor map and all pixels on plastics fragments are well identified from a single color selection the phasor map. From their position in the phasor plot it is possible to infer that analogous photophysical processes are involved in LDPE PS and PET decays. The phasor corresponding to LDPE lies on the universal circle

340 indicating that Nile Red Lifetime is a single exponential ($\tau$ = 3.1 ns). The observed
341 behavior may arise from a progressive decrease of the contribution of the higher energy
342 state due to spectral relaxation mechanisms which can be ascribed to the increased
343 polarity of Nile Red environment. Fluorescence lifetime distribution for Nylon samples
344 describe a different panorama, reflecting critically different chemical composition. The
345 quantitative detailed explanation of this behavior is certainly of great interest and needs
346 further studies, but it is out from the scope of this work. We here demonstrated that
347 lifetime distribution position in the phasor plot constitute a fingerprint of plastic nature
348 allowing to recognize them, quickly and easily in water environment. This is also possible
349 if different microplastics are simultaneously present in the same sample as shown in
350 Figure 7 (where a mosaic collection of images is shown to enhance the field of view).
351 Using the very same selections as the ones reported above, different microplastics are
352 quickly identified in the same images. Structures colored in green are identified as LDPE
353 MPs, this being also confirmed by their morphology, PS and PET are colored in yellow
354 and pink respectively and Nylon is colored in red.

355

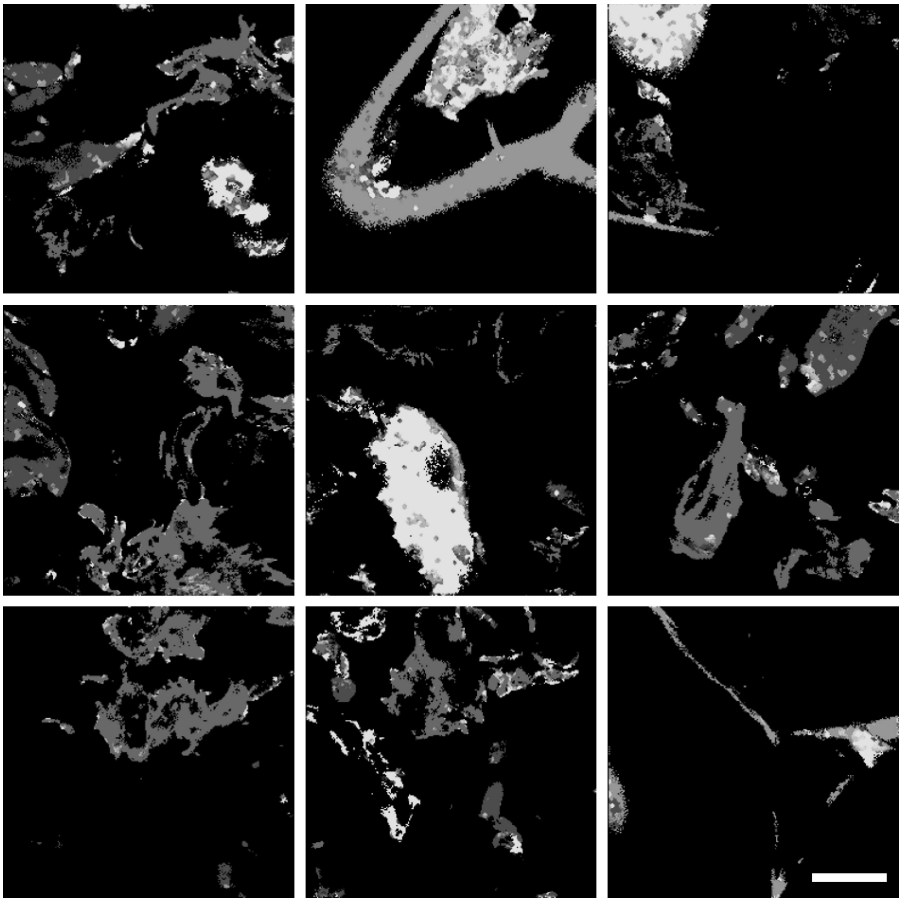

**Figure 7.** *Detection and identification of different Microplastics. Representative images of a mixture of microplastics simultaneously detected and colored according to the color code defined in the phasor plot reported in Figure6: LDPE (green), PS (yellow) PET (pink) and Nylon (red). Scale bar is 200 µm.*

## Conclusions.

In the last decade, the detection and the analysis of microplastics have become of utmost importance since they are becoming a real risk for the ecosystem and, as a consequence, for human health.

In this article, we report on a microplastics Nile Red fluorescence lifetime analysis that provides a simple and sensitive approach in detecting different widespread used plastics.

368 The analysis was performed on microplastics attained by a simple surface Nile Red
369 staining protocol performed in aqueous environment that is relatively fast and does not
370 require complex chemical procedures or separation processes. Significant differences
371 were observed in the emission spectrum and, most importantly, in the fluorescence
372 lifetime. Specifically, results showed that the fluorescence emission spectra and lifetime
373 of Nile Red are sensible to polymer matrix providing a fingerprint for the identification
374 of fragments from different types of polymers. Fluorescence lifetime imaging (FLIM)
375 coupled with Nile Red staining allows a direct visualization and localization of
376 microplastics, they can be easy quantified in terms of size, morphology. Moreover, FLIM
377 analysis using phasor approach allows quantitative interpretation of the data and the
378 straightforward identification of multiple coexisting microplastics species in the same
379 sample.

380 We presented the proof of concept of a new approach based on confocal fluorescence
381 microscopy which allows simple, fast non-invasive acquisition of optical sections of thick
382 samples at high resolution (down to 200 nm) that can be readily adapted to measure
383 microplastics samples in seawater and opens new perspectives in this field. Further
384 studies extended to other plastics and in the presence of different additives, metals or
385 chemical modifications may open new perspectives in the characterisation of MPs and to
386 extend the amount of accessible information. Additional future developments could foster
387 Nile Red fluorescence lifetime imaging by combining this approach with other advanced
388 imaging systems to allow identification, localization and tracking of individual types of
389 microplastics (and nanoplastics) from (sub) cellular level [65,66] to whole organ [67–69]
390 such as brain and neural system [70–73]. We envisage a future step toward the detection
391 of Nanoplastics by using super-resolution optical methods (i.e. Stimulated Emission

392 Depletion (STED) microscopy) [74] that, coupled to fluorescence lifetime analysis [75],
393 may provide a suitable tool for Nanoplastics localization and analysis.

394

395 REFERENCES


396 1. Akdogan Z, Guven B. Microplastics in the environment: A critical review of current
397 understanding and identification of future research needs. Environmental Pollution.
398 2019. doi:10.1016/j.envpol.2019.113011

399 2. Zhang Y, Gao T, Kang S, Sillanpää M. Importance of atmospheric transport for
400 microplastics deposited in remote areas. Environmental Pollution. 2019.
401 doi:10.1016/j.envpol.2019.07.121

402 3. Kanhai LDK, Gardfeldt K, Krumpen T, Thompson RC, O'Connor I. Microplastics in sea
403 ice and seawater beneath ice floes from the Arctic Ocean. Sci Rep. 2020;10.
404 doi:10.1038/s41598-020-61948-6

405 4. Prata JC. Airborne microplastics: Consequences to human health? Environmental
406 Pollution. 2018. pp. 115–126. doi:10.1016/j.envpol.2017.11.043

407 5. Seeley ME, Song B, Passie R, Hale RC. Microplastics affect sedimentary microbial
408 communities and nitrogen cycling. Nat Commun. 2020;11. doi:10.1038/s41467-020-
409 16235-3

410 6. Brennecke D, Duarte B, Paiva F, Caçador I, Canning-Clode J. Microplastics as vector
411 for heavy metal contamination from the marine environment. Estuar Coast Shelf Sci.
412 2016;178: 189–195. doi:10.1016/j.ecss.2015.12.003

413 7. Jambeck JR, Geyer R, Wilcox C, Siegler TR, Perryman M, Andrady A, et al. Plastic
414 waste inputs from land into the ocean. Science (80- ). 2015;347: 768–771.
415 doi:10.1126/science.1260352

416 8. Auta HS, Emenike CU, Fauziah SH. Distribution and importance of microplastics in the
417 marine environmentA review of the sources, fate, effects, and potential solutions.
418 Environment International. 2017. doi:10.1016/j.envint.2017.02.013

419 9. Cole M, Webb H, Lindeque PK, Fileman ES, Halsband C, Galloway TS. Isolation of
420 microplastics in biota-rich seawater samples and marine organisms. Sci Rep. 2014;4.
421 doi:10.1038/srep04528

10. Thompson RC, Olson Y, Mitchell RP, Davis A, Rowland SJ, John AWG, et al. Lost at Sea: Where Is All the Plastic? Science (80- ). 2004;304: 838. doi:10.1126/science.1094559

11. Barboza LGA, Dick Vethaak A, Lavorante BRBO, Lundebye AK, Guilhermino L. Marine microplastic debris: An emerging issue for food security, food safety and human health. Marine Pollution Bulletin. 2018. pp. 336–348. doi:10.1016/j.marpolbul.2018.05.047

12. Hartmann NB, Rist S, Bodin J, Jensen LHS, Schmidt SN, Mayer P, et al. Microplastics as vectors for environmental contaminants: Exploring sorption, desorption, and transfer to biota. Integrated Environmental Assessment and Management. 2017. pp. 488–493. doi:10.1002/ieam.1904

13. Holmes LA, Turner A, Thompson RC. Adsorption of trace metals to plastic resin pellets in the marine environment. Environ Pollut. 2012;160: 42–48. doi:10.1016/j.envpol.2011.08.052

14. Galloway TS. Micro- and nano-plastics and human health. Marine Anthropogenic Litter. 2015. pp. 343–366. doi:10.1007/978-3-319-16510-3_13

15. Hwang J, Choi D, Han S, Jung SY, Choi J, Hong J. Potential toxicity of polystyrene microplastic particles. Sci Rep. 2020;10. doi:10.1038/s41598-020-64464-9

16. Sharma S, Chatterjee S. Microplastic pollution, a threat to marine ecosystem and human health: a short review. Environ Sci Pollut Res. 2017;24: 21530–21547. doi:10.1007/s11356-017-9910-8

17. Kögel T, Bjorøy Ø, Toto B, Bienfait AM, Sanden M. Micro- and nanoplastic toxicity on aquatic life: Determining factors. Science of the Total Environment. 2020. doi:10.1016/j.scitotenv.2019.136050

18. Lee WS, Cho HJ, Kim E, Huh YH, Kim HJ, Kim B, et al. Bioaccumulation of polystyrene nanoplastics and their effect on the toxicity of Au ions in zebrafish embryos. Nanoscale. 2019;11: 3200–3207. doi:10.1039/c8nr09321k

19. Rochman CM, Kurobe T, Flores I, Teh SJ. Early warning signs of endocrine disruption in adult fish from the ingestion of polyethylene with and without sorbed chemical pollutants from the marine environment. Sci Total Environ. 2014;493: 656–661. doi:10.1016/j.scitotenv.2014.06.051

20. Kim D, Chae Y, An YJ. Mixture Toxicity of Nickel and Microplastics with Different

Functional Groups on Daphnia magna. Environ Sci Technol. 2017;51: 12852–12858. doi:10.1021/acs.est.7b03732

21. Rochman CM, Hoh E, Hentschel BT, Kaye S. Long-term field measurement of sorption of organic contaminants to five types of plastic pellets: Implications for plastic marine debris. Environ Sci Technol. 2013;47: 1646–1654. doi:10.1021/es303700s

22. Bilotta GS, Brazier RE. Understanding the influence of suspended solids on water quality and aquatic biota. Water Research. 2008. pp. 2849–2861. doi:10.1016/j.watres.2008.03.018

23. Hidalgo-Ruz V, Gutow L, Thompson RC, Thiel M. Microplastics in the marine environment: A review of the methods used for identification and quantification. Environ Sci Technol. 2012;46: 3060–3075. doi:10.1021/es2031505

24. Lavers JL, Oppel S, Bond AL. Factors influencing the detection of beach plastic debris. Mar Environ Res. 2016;119: 245–251. doi:10.1016/j.marenvres.2016.06.009

25. Shim WJ, Hong SH, Eo SE. Identification methods in microplastic analysis: A review. Analytical Methods. 2017. pp. 1384–1391. doi:10.1039/c6ay02558g

26. Song YK, Hong SH, Jang M, Han GM, Rani M, Lee J, et al. A comparison of microscopic and spectroscopic identification methods for analysis of microplastics in environmental samples. Mar Pollut Bull. 2015;93: 202–209. doi:10.1016/j.marpolbul.2015.01.015

27. Desforges JPW, Galbraith M, Ross PS. Ingestion of Microplastics by Zooplankton in the Northeast Pacific Ocean. Arch Environ Contam Toxicol. 2015;69. doi:10.1007/s00244-015-0172-5

28. Ivleva NP, Wiesheu AC, Niessner R. Microplastic in Aquatic Ecosystems. Angewandte Chemie - International Edition. 2017. pp. 1720–1739. doi:10.1002/anie.201606957

29. Harrison JP, Ojeda JJ, Romero-González ME. The applicability of reflectance micro-Fourier-transform infrared spectroscopy for the detection of synthetic microplastics in marine sediments. Sci Total Environ. 2012;416: 455–463. doi:10.1016/j.scitotenv.2011.11.078

30. Tagg AS, Sapp M, Harrison JP, Ojeda JJ. Identification and Quantification of Microplastics in Wastewater Using Focal Plane Array-Based Reflectance Micro-FT-IR Imaging. Anal Chem. 2015;87: 6032–6040. doi:10.1021/acs.analchem.5b00495

31. Chen Y, Wen D, Pei J, Fei Y, Ouyang D, Zhang H, et al. Identification and quantification of microplastics using Fourier-transform infrared spectroscopy: Current status and future prospects. Current Opinion in Environmental Science and Health. 2020. pp. 14–19. doi:10.1016/j.coesh.2020.05.004

32. Fries E, Dekiff JH, Willmeyer J, Nuelle MT, Ebert M, Remy D. Identification of polymer types and additives in marine microplastic particles using pyrolysis-GC/MS and scanning electron microscopy. Environ Sci Process Impacts. 2013;15: 1949–1956. doi:10.1039/c3em00214d

33. Käppler A, Windrich F, Löder MGJ, Malanin M, Fischer D, Labrenz M, et al. Identification of microplastics by FTIR and Raman microscopy: a novel silicon filter substrate opens the important spectral range below 1300 cm−1 for FTIR transmission measurements. Anal Bioanal Chem. 2015;407. doi:10.1007/s00216-015-8850-8

34. Pawley JB. Confocal and two-photon microscopy: Foundations, applications and advances. Microsc Res Tech. 2002;59: 148–149. doi:10.1002/jemt.10188

35. Diaspro A. Super-Resolution Imaging in Biomedicine. Super-Resolution Imaging in Biomedicine. 2016. doi:10.4324/9781315372884

36. Lakowicz JR. Principles of fluorescence spectroscopy. Principles of Fluorescence Spectroscopy. 2006. doi:10.1007/978-0-387-46312-4

37. Erni-Cassola G, Gibson MI, Thompson RC, Christie-Oleza JA. Lost, but Found with Nile Red: A Novel Method for Detecting and Quantifying Small Microplastics (1 mm to 20 μm) in Environmental Samples. Environ Sci Technol. 2017;51: 13641–13648. doi:10.1021/acs.est.7b04512

38. Maes T, Jessop R, Wellner N, Haupt K, Mayes AG. A rapid-screening approach to detect and quantify microplastics based on fluorescent tagging with Nile Red. Sci Rep. 2017;7. doi:10.1038/srep44501

39. Mason SA, Welch VG, Neratko J. Synthetic Polymer Contamination in Bottled Water. Front Chem. 2018;6. doi:10.3389/fchem.2018.00407

40. Prata JC, Alves JR, da Costa JP, Duarte AC, Rocha-Santos T. Major factors influencing the quantification of Nile Red stained microplastics and improved automatic quantification (MP-VAT 2.0). Sci Total Environ. 2020;719. doi:10.1016/j.scitotenv.2020.137498

41. Prata JC, Reis V, Matos JTV, da Costa JP, Duarte AC, Rocha-Santos T. A new approach

for routine quantification of microplastics using Nile Red and automated software (MP-VAT). Sci Total Environ. 2019;690: 1277–1283. doi:10.1016/j.scitotenv.2019.07.060

42. Shim WJ, Song YK, Hong SH, Jang M. Identification and quantification of microplastics using Nile Red staining. Mar Pollut Bull. 2016;113: 469–476. doi:10.1016/j.marpolbul.2016.10.049

43. Greenspan P, Mayer EP, Fowler SD. Nile red: A selective fluorescent stain for intracellular lipid droplets. J Cell Biol. 1985;100: 965–973. doi:10.1083/jcb.100.3.965

44. Sackett DL, Wolff J. Nile red as a polarity-sensitive fluorescent probe of hydrophobic protein surfaces. Anal Biochem. 1987;167: 228–234. doi:10.1016/0003-2697(87)90157-6

45. Greenspan P, Fowler SD. Spectrofluorometric studies of the lipid probe, nile red. J Lipid Res. 1985;26: 781–789.

46. Dutta AK, Kamada K, Ohta K. Spectroscopic studies of nile red in organic solvents and polymers. J Photochem Photobiol A Chem. 1996;93: 57–64. doi:10.1016/1010-6030(95)04140-0

47. Hengstmann E, Fischer EK. Nile red staining in microplastic analysis—proposal for a reliable and fast identification approach for large microplastics. Environ Monit Assess. 2019;191. doi:10.1007/s10661-019-7786-4

48. Tamminga M. Nile Red Staining as a Subsidiary Method for Microplastic Quantification: A Comparison of Three Solvents and Factors Influencing Application Reliability. SDRP J Earth Sci Environ Stud. 2017;2. doi:10.15436/jeses.2.2.1

49. Cser A, Nagy K, Biczók L. Fluorescence lifetime of Nile Red as a probe for the hydrogen bonding strength with its microenvironment. Chem Phys Lett. 2002;360: 473–478. doi:10.1016/S0009-2614(02)00784-4

50. Hess CM, Riley EA, Reid PJ. Dielectric dependence of single-molecule photoluminescence intermittency: Nile red in poly(vinylidene fluoride). J Phys Chem B. 2014;118: 8905–8913. doi:10.1021/jp505874m

51. Stringari C, Cinquin A, Cinquin O, Digman MA, Donovan PJ, Gratton E. Phasor approach to fluorescence lifetime microscopy distinguishes different metabolic states of germ cells in a live tissue. Proc Natl Acad Sci U S A. 2011;108: 13582–13587. doi:10.1073/pnas.1108161108

548 52. Digman MA, Caiolfa VR, Zamai M, Gratton E. The phasor approach to fluorescence
549 lifetime imaging analysis. Biophys J. 2008;94. doi:10.1529/biophysj.107.120154

550 53. Worrell E, Reuter MA. Handbook of Recycling: State-of-the-art for Practitioners,
551 Analysts, and Scientists. Handbook of Recycling: State-of-the-art for Practitioners,
552 Analysts, and Scientists. 2014. doi:10.1016/C2011-0-07046-1

553 54. Campo EA. Polymeric Materials and Properties. Selection of Polymeric Materials. 2008.
554 pp. 1–39. doi:10.1016/b978-081551551-7.50003-6

555 55. Sarkar N, Das K, Nath DN, Bhattacharyya K. Twisted Charge Transfer Process of Nile
556 Red in Homogeneous Solution and in Faujasite Zeolite. Langmuir. 1994;10: 326–329.
557 doi:10.1021/la00013a048

558 56. Mataga N, Kaifu Y, Koizumi M. Solvent Effects upon Fluorescence Spectra and the
559 Dipolemoments of Excited Molecules. Bull Chem Soc Jpn. 1956;29: 465–470.
560 doi:10.1246/bcsj.29.465

561 57. Ma N, Digman MA, Malacrida L, Gratton E. Measurements of absolute concentrations
562 of NADH in cells using the phasor FLIM method. Biomed Opt Express. 2016;7: 2441.
563 doi:10.1364/boe.7.002441

564 58. Harvey BJ, Levitus M. Nucleobase-specific enhancement of Cy3 fluorescence. J
565 Fluoresc. 2009;19: 443–448. doi:10.1007/s10895-008-0431-1

566 59. Malacrida L, Jameson DM, Gratton E. A multidimensional phasor approach reveals
567 LAURDAN photophysics in NIH-3T3 cell membranes. Sci Rep. 2017;7.
568 doi:10.1038/s41598-017-08564-z

569 60. Levitt JA, Chung P-H, Suhling K. Spectrally resolved fluorescence lifetime imaging of
570 Nile red for measurements of intracellular polarity. J Biomed Opt. 2015;20: 096002.
571 doi:10.1117/1.jbo.20.9.096002

572 61. De Luca G, Fennema Galparsoro D, Sancataldo G, Leone M, Foderà V, Vetri V. Probing
573 ensemble polymorphism and single aggregate structural heterogeneity in insulin amyloid
574 self-assembly. J Colloid Interface Sci. 2020;574: 229–240.
575 doi:10.1016/j.jcis.2020.03.107

576 62. Sancataldo G, Anselmo S, Vetri V. Phasor-FLIM analysis of Thioflavin T self-
577 quenching in Concanavalin amyloid fibrils. Microsc Res Tech. 2020;83: 811–816.
578 doi:10.1002/jemt.23472

63. Sartorio C, Giuliano G, Scopelliti M, Vetri V, Leone M, Pignataro B. Synergies and compromises between charge and energy transfers in three-component organic solar cells. Phys Chem Chem Phys. 2020;22: 8344–8352. doi:10.1039/d0cp00336k

64. Sartorio C, Scaramuzza S, Cataldo S, Vetri V, Scopelliti M, Leone M, et al. Donor-Acceptor Interfaces by Engineered Nanoparticles Assemblies for Enhanced Efficiency in Plastic Planar Heterojunction Solar Cells. J Phys Chem C. 2016;120: 26588–26599. doi:10.1021/acs.jpcc.6b07302

65. Sancataldo G, Scipioni L, Ravasenga T, Lanzanò L, Diaspro A, Barberis A, et al. Three-dimensional multiple-particle tracking with nanometric precision over tunable axial ranges. Optica. 2017;4: 367. doi:10.1364/optica.4.000367

66. Duocastella M, Sancataldo G, Saggau P, Ramoino P, Bianchini P, Diaspro A. Fast Inertia-Free Volumetric Light-Sheet Microscope. ACS Photonics. 2017;4: 1797–1804. doi:10.1021/acsphotonics.7b00382

67. D'Amora M, Rodio M, Sancataldo G, Diaspro A, Intartaglia R. Laser-Fabricated Fluorescent, Ligand-Free Silicon Nanoparticles: Scale-up, Biosafety, and 3D Live Imaging of Zebrafish under Development. ACS Appl Bio Mater. 2019;2: 321–329. doi:10.1021/acsabm.8b00609

68. D'Amora M, Rodio M, Bartelmess J, Sancataldo G, Brescia R, Cella Zanacchi F, et al. Biocompatibility and biodistribution of functionalized carbon nano-onions (f-CNOs) in a vertebrate model. Sci Rep. 2016;6. doi:10.1038/srep33923

69. Lavagnino Z, Sancataldo G, D'Amora M, Follert P, De Pietri Tonelli D, Diaspro A, et al. 4D (x-y-z-t) imaging of thick biological samples by means of Two-Photon inverted Selective Plane Illumination Microscopy (2PE-iSPIM). Sci Rep. 2016;6. doi:10.1038/srep23923

70. Sancataldo G, Silvestri L, Allegra Mascaro AL, Sacconi L, Pavone FS. Advanced fluorescence microscopy for in vivo imaging of neuronal activity. Optica. 2019;6: 758. doi:10.1364/optica.6.000758

71. Sancataldo G, Gavryusev V, de Vito G, Turrini L, Locatelli M, Fornetto C, et al. Flexible multi-beam light-sheet fluorescence microscope for live imaging without striping artifacts. Front Neuroanat. 2019;13. doi:10.3389/fnana.2019.00007

72. Gavryusev V, Sancataldo G, Ricci P, Montalbano A, Fornetto C, Turrini L, et al. Dual-beam confocal light-sheet microscopy via flexible acousto-optic deflector. J Biomed

Opt. 2019;24: 1. doi:10.1117/1.jbo.24.10.106504

73. Ricci P, Sancataldo G, Gavryusev V, Franceschini A, Müllenbroich MC, Silvestri L, et al. Fast multi-directional DSLM for confocal detection without striping artifacts. Biomed Opt Express. 2020;11: 3111. doi:10.1364/boe.390916

74. Hell SW, Wichmann J. Breaking the diffraction resolution limit by stimulated emission: stimulated-emission-depletion fluorescence microscopy. Opt Lett. 1994;19: 780. doi:10.1364/ol.19.000780

75. Auksorius E, Boruah BR, Dunsby C, Lanigan PMP, Kennedy G, Neil MAA, et al. Stimulated emission depletion microscopy with a supercontinuum source and fluorescence lifetime imaging. Opt Lett. 2008;33: 113. doi:10.1364/ol.33.000113

## AUTHOR INFORMATION

### Corresponding Author

giuseppe.sancataldo@unipa.it

### Author Contributions

GS and VV developed the idea behind the project and designed the experiments. GS, VV and GA discussed results. GS performed the experiments and analyzed the data. VV and GS wrote the manuscript. All authors contributed to the writing of the manuscript and approved the final version of the manuscript.

### Funding Sources

This project has received funding from PON AIM1809078-1

### Acknowledgements

Authors acknowledge the ‘Molecular Biophysics and Nanotechnologies’ group and especially prof. Maurizio Leone for helpful suggestions and discussions.

## Notes

The authors declare no conflict of interest.

## ASSOCIATED CONTENT

**Supplementary Information**. Supporting video on graphical phasor analysis of two population of microplastics using simFCS.